SIMULATION AND EXPERIMENTAL STUDIES OF INTAKE AND EXHAUST TUNING FOR AUTOMOTIVE ENGINE LOW-END TORQUE ENHANCEMENT

KHOO AIK SOON

UNIVERSITI SAINS MALAYSIA

2014

SIMULATION AND EXPERIMENTAL STUDIES OF INTAKE AND EXHAUST TUNING FOR AUTOMOTIVE ENGINE LOW-END TORQUE ENHANCEMENT

by

KHOO AIK SOON

Thesis submitted in fulfillment of the
requirements for the degree of
Master of Science

September 2014

ACKNOWLEDGEMENT

This thesis is the end of my journey in doing my Master study. It is a pleasure to thank those who have assisted me a lot during the journey.

I am deeply grateful to my supervisors, Professor Horizon Walker Gitano-Briggs and Professor Zainal Alimuddin bin Zainal Alauddin, for giving me important guidance and supports at key moment in my work. Without them this work would not have been possible. Thank you does not seem sufficient but it is said with appreciation and respect.

I wish to extend my warmest thank to Mr. Zalmi bin Yop and the technical staffs, for not letting me down whenever I need assistance in fabrication works. I also acknowledge Universiti Sains Malaysia for providing me a good research environment and financial support from USM fellowship scheme.

Not to forget to express my appreciation to my colleagues in Engine Laboratory for their insightful comments and discussions. Thank them for giving helping hand during their busy time and helped to make the university life an easygoing challenge.

Lastly and most importantly, I wish to thank my family members and friends, for their loving support. For my parent, thank for giving me freedom to pursue my dreams even sometimes it appear to be incomprehensible or dangerous.

TABLE OF CONTENTS

ACKNOWLEDGEMENT ii

TABLE OF CONTENTS iii

LIST OF FIGURES viii

LIST OF TABLES xv

LIST OF ABBREVIATIONS AND SYMBOLS xvi

ABSTRAK xvii

ABSTRACT xviii

CHAPTER 1 INTRODUCTION 1

1.1 Research Background 1

1.2 Low-End Torque 3

1.3 Problem Statement 5

1.4 Objectives 6

1.5 Scope of Research 6

CHAPTER 2 LITERATURE REVIEW 8

2.1 Overview 8

2.2 Solutions for Low-End Torque 8

  2.2.1 Forced Induction 8

  2.2.2 Valve Timing and Lift Profile 10

  2.2.3 Manifold Tuning 11

2.3 Manifold Tuning Background 12

2.4 Pressure Wave 13

    2.4.1 Pressure Wave's Motion in Pipe 13

    2.4.2 Wave Propagation Velocity and Gas Particle Velocity 14

2.5 Pressure Wave Reflection 16

    2.5.1 Pressure Wave Reflection at the Open End of a Pipe 17

    2.5.2 Pressure Wave Reflection at the Closed End of a Pipe 17

    2.5.3 Pressure Wave Reflection at Sudden Area Change 18

    2.5.4 Pressure Wave Reflection at Branches of Pipe 21

2.6 Intake Tuning 23

2.7 Exhaust Tuning 27

2.8 Summary 34

CHAPTER 3 METHODOLOGY 35

3.1 Overview 35

3.2 Engine Selection and Specifications 35

3.3 Engine Test Cell and Instrumentations 38

    3.3.1 Dynamometer Controller 40

    3.3.2 Fuel Measurement 40

    3.3.3 Manifold Pressure Measurement 41

        3.3.3 (a) Pressure Sensor 42

        3.3.3 (b) Crankshaft Position Encoder 42

3.3.3 (c) Data Acquisition Unit 43

3.3.4 Temperature, Pressure and Relative Humidity Measurement 44

3.4 Data Recording 45

3.5 Test Procedure 46

3.6 Data Processing 49

3.6.1 Dynamometer Correction Factor 49

3.6.2 Manifold Pressure Data Processing 51

3.7 Engine Modelling 52

3.7.1 Geometric Data 55

3.7.2 Engine Data 57

3.7.2 (a) Mechanical Friction Properties 58

3.7.2 (b) Combustion Properties 59

3.7.2 (c) Valves Properties 61

3.7.3 Operating Parameters 63

3.7.4 Parts That Require Special Modelling Technique 64

3.7.4 (a) Air Filter 64

3.7.4 (b) Catalytic Converter 65

3.7.4 (c) Cat-Back 66

3.7.4 (d) Valve Timing Investigation 67

3.7.4 (e) Y-Junction - Duct Connection with Abrupt Change of Diameter 68

3.8 Parametric Study and Engine Model Utilisation 70

3.9 Engine Modifications 71

3.9.1 Intake System 72

3.9.2 Exhaust System 74

CHAPTER 4 RESULTS AND DISCUSSION 76

4.1 Overview 76

4.2 Engine Model Validation.. 76

4.2.1 Proton Experimental vs Wave Simulation 76

4.2.2 Proton Experimental vs USM Experimental (Baseline Data) 80

4.2.3 USM Experimental vs Wave Simulation (Manifold Pressure Trace) 82

4.3 Original System Analysis 84

4.4 Exhaust Tuning.. 87

4.4.1 Exhaust System Configuration 88

4.4.2 Exhaust Runner Length 90

4.4.3 4-2-1 Exhaust Header 93

4.4.3 (a) Simulated Engine Torque 94

4.4.3 (b) Experimental Result of Engine Torque and Intake Pressure... 94

4.4.3 (c) System Analysis by Simulation Model 97

4.5 Intake Tuning.. 104

4.5.1 Intake Runner Diameter 104

4.5.2 Intake Runner Length.. 110

4.6 Combination of Intake and Exhaust Tuning 115

CHAPTER 5 CONCLUSIONS 117

5.1 Conclusions 117

5.2 Future Works 118

REFERENCES 120

APPENDICES

Appendix A Malaysia Top 10 Car Models and Corresponding Engine Specifications (Jan-Apr 2012)

Appendix B Schenck W130 Characteristic Curve

Appendix C MPX5500DP Pressure Sensor

Appendix D SAE J1349 Standard

Appendix E Source Code of C++ Programming

LIST OF FIGURES

Figure 1.1: Share of gasoline engines' displacement ranges in liters (Arif Basheer 2010). 3

Figure 1.2: Performance map for 2 liter 4 cylinders SI engine (Heywood 1988). 4

Figure 1.3: Motored FMEP vs. engine speed of a 4 cylinders SI engine (Heywood 1988). 5

Figure 2.1: Pressure waves propagation in pipe (Blair 1999). 14

Figure 2.2: Pressure wave reflection at open end (Winterbone & Nichols 1985)... 17

Figure 2.3: Pressure wave reflection at closed end (Winterbone & Nichols 1985). 18

Figure 2.4: Sudden expansion and sudden contraction in pipe flow (Blair 1999). 19

Figure 2.5: Pressure wave propagation at 3-way branch (Blair 1999). 22

Figure 2.6: Computed intake pressure for optimal intake length at each engine speed (Vitek & Polasek 2002). 25

Figure 2.7: Volumetric efficiency vs. intake pressure at IVC (Hamilton et al. 2009). 25

Figure 2.8: Brake torque vs. speed of new intake and original intake system (Pai et al. 2011). 26

Figure 2.9: Overlapping of later stage of exhaust stroke on cylinder 1 with beginning stage of exhaust stroke on cylinder 3. 29

Figure 2.10: Exhaust pipe arrangements for inline 4-cylinders engine: A. 4-1 collector B. 360° Tri-Y collector C. 180° Tri-Y collector 30

Figure 2.11: Engine performance with different exhaust manifold arrangement (Jawad et al. 2002). 31

Figure 2.12: Engine torque comparison between baseline production and improved low-speed system (Bush et al. 2000). 32

Figure 2.13: Engine power and torque comparison of 2001 and 2002 exhaust system (Jawad et al. 2002). 33

Figure 3.1: Intake cam lobes for CPS cam shaft; low lift cam on center, high lift cam on both sides. 36

Figure 3.2: Valve lift profiles of Campro CPS engine (Proton Powertrain 2003). 37

Figure 3.3: Cross sectional view of intake manifold; long tract and short tract intakes (Proton Powertrain 2003). 37

Figure 3.4: Schematic diagram of engine test bed. 38

Figure 3.5: Extended frame test bed with test engine on it. 39

Figure 3.6: Fuel measurement system. 41

Figure 3.7: Manifold pressure data acquisition system. 41

Figure 3.8: Exhaust manifold, copper tube and plastic hose for pressure measurement. 42

Figure 3.9: Overview of data acquisition system. 43

Figure 3.10: Mercury J-tube barometer for ambient pressure measurement. 44

Figure 3.11: Agilent VEE program layout for engine testing. 45

Figure 3.12: Flow chart for A. performance test and B. pressure traces measurement testing procedure. 48

Figure 3.13: Campro CPS engine model in WaveBuild GUI. 54

Figure 3.14: Intake manifold model was generated by WaveMesher from 3D CAD drawing. 56

Figure 3.15: PTrAn screenshot: cumulative mass fraction burned curve (bottom) was generated from input cylinder pressure profile (above). 61

Figure 3.16: Flow bench model in WAVE.. 62

Figure 3.17: Experimental and simulated volume flow rate of flow bench. 63

Figure 3.18: Original C_f and fine tuned C_f. 63

Figure 3.19: WAVE model for air filter calibration.. 65

Figure 3.20: Catalytic converter 66

Figure 3.21: Exhaust back pressure of experimental and simulation data. 67

Figure 3.22: Experimental torque curve with predicted torque curves before and after cam lobe center adjustment. 68

Figure 3.23: Taper duct has been used to model abrupt change in diameter at Y-junction and duct connection. 69

Figure 3.24: Volumetric efficiency of model with original approach and taper duct approach 70

Figure 3.25: Original model and modified model with additional test points. 71

Figure 3.26: Original intake system. 73

Figure 3.27: Fabricated straight intake manifold with 50mm & 100mm length flanges. 73

Figure 3.28: Original exhaust system. 74

Figure 3.29: 4-2-1 exhaust header. 75

Figure 4.1: Torque curve of Proton data and WAVE data. 77

Figure 4.2: Volumetric efficiency of Proton data and WAVE data. 77

Figure 4.3: Maximum combustion pressure and its location of Proton data and WAVE data. 78

Figure 4.4: Simulated and experimental combustion pressure trace at 3500rpm. .. 79

Figure 4.5: BSFC of Proton data and WAVE data.. 80

Figure 4.6: Experimental torque and BSFC curve of USM and Proton baseline data.. 81

Figure 4.7: Fuel consumption and percentage difference of USM baseline and Proton data. 82

Figure 4.8: Intake manifold pressure trace (sensor location) at 3500rpm; experimental vs. WAVE. 83

Figure 4.9: Exhaust manifold pressure trace (sensor location) at 3500rpm; experimental vs. WAVE. 84

Figure 4.10: Simulated pressure and mass flow rate of original system at intake and exhaust ports; 3500rpm. 85

Figure 4.11: Simulated pressure and mass flow rate of original system at intake and exhaust ports; 3000rpm. 86

Figure 4.12: Simulated pressure and mass flow rate of original system at intake and exhaust ports; 2500rpm. 87

Figure 4.13: Simulated exhaust pressure of original system at each cylinder’s exhaust port. 89

Figure 4.14: Simulated exhaust pressure from each cylinder of 4-2-1 header with 360° Tri-Y collector. 89

Figure 4.15: Simulated data of different primary exhaust runner length. 91

Figure 4.16: Simulated data of exhaust system of 500mm primary runner length addition at 3500rpm; pressure and mass flow rate at intake and exhaust ports. 93

Figure 4.17: Simulation result for 4-2-1 header. 94

Figure 4.18: Measured torque of 4-2-1 exhaust header compare to baseline result. 95

Figure 4.19: Measured intake pressure of original system and 4-2-1 header at sensor location; 2500rpm. 96

Figure 4.20: Measured intake pressure of original system and 4-2-1 header at sensor location; 3000rpm. 96

Figure 4.21: Measured intake pressure of original system and 4-2-1 header at sensor location; 3500rpm. 97

Figure 4.22: Simulated intake and exhaust port pressure for original and 4-2-1 exhaust header 2500rpm. 98

Figure 4.23: Simulated intake and exhaust port pressure for original and 4-2-1 exhaust header 3000rpm. 98

Figure 4.24: Simulated intake and exhaust port pressure for original and 4-2-1 exhaust header 3500rpm. 99

Figure 4.25: Simulated intake and exhaust mass flow rate for original and 4-2-1 exhaust header 2500rpm. 100

Figure 4.26: Simulated intake and exhaust mass flow rate for original and 4-2-1 exhaust header 3000rpm. 100

Figure 4.27: Simulated intake and exhaust mass flow rate for original and 4-2-1 exhaust header 3500rpm. 101

Figure 4.28: Predicted volumetric efficiency and residual gas fraction of original system and 4-2-1 header. 102

Figure 4.29: Calculated pressure traces and valve lift profiles vs. crank angle at 13000rpm (Badami et al. 2002). 103

Figure 4.30: Calculated mass flow rates and valve lift profiles vs. crank angle at 13000rpm (Badami et al. 2002). 103

Figure 4.31: Simulation results of intake diameter × 0.8; predicted torque and percentage difference. 105

Figure 4.32: Simulation results of intake diameter × 0.9; predicted torque and percentage difference. 105

Figure 4.33: Simulation results of intake diameter × 1.1; predicted torque and percentage difference. 106

Figure 4.34: Simulation results of intake diameter × 1.2; predicted torque and percentage difference. 106

Figure 4.35: Simulation results of straight intake with runner diameter of 38mm and 35.5mm; predicted torque and percentage difference. 107

Figure 4.36: Experimental torque curves of USM baseline, 38mm and 35.5mm diameter straight intake runners. 108

Figure 4.37: Simulated intake pressure and mass flow rate at intake port for straight intake runner with 38mm and 35.5mm diameter at 2500rpm. 109

Figure 4.38: Simulation results of intake length × 0.8; predicted torque and percentage difference. 110

Figure 4.39: Simulation results of intake length × 0.9; predicted torque and percentage difference. 111

Figure 4.40: Simulation results of intake length × 1.1; predicted torque and percentage difference. 111

Figure 4.41: Simulation results of intake length × 1.2; predicted torque and percentage difference. 112

Figure 4.42: Predicted torque of straight intake manifold with different runner length from 550mm to 700mm. 113

Figure 4.43: Experimental results for varying intake length. 113

Figure 4.44: Simulated intake pressure and mass flow rate at intake port of straight intake manifold with 600mm and 700mm runner length at 2500rpm. 114

Figure 4.45: Measured torque curves of baseline and tuned manifold system. 116

LIST OF TABLES

Table 1.1: Road tax rate of individually owned motocar in Peninsular Malaysia 2

Table 1.2: Proton Exora engine speed at corresponding vehicle speed 4

Table 3.1: Campro CPS engine technical specifications 36

Table 3.2: Cam profile and intake manifold configurations 38

Table 3.3: Reference atmospheric condition in SAE J1349 standard 50

Table 4.1: Predicted torque, volumetric efficiency and residual gas fraction of original and 500mm longer exhaust system at 3500rpm. 93

Table 4.2: Pressure at IVC and percentage of back flow for 600mm and 700mm straight intake runner. 115

LIST OF ABBREVIATIONS AND SYMBOLS

ACF	Air correction factor
AFR	Air fuel ratio
AMM	Agilent Measurement Manager
BSFC	Brake specific fuel consumption
CPS	Cam profile switching
CSV	Comma-separated values
DAQ	Data acquisition unit
DOHC	Double overhead cam
ECF	Engine correction factor
ECU	Engine control unit
EV	Exhaust valves
EVC	Exhaust valves close
EVO	Exhaust valves open
EXPT	Experimental
GUI	Graphical user interface
ICE	Internal combustion engine
IV	Intake valves
IVC	Intake valves close
IVO	Intake valves open
LHV	Lower heating value
PTO	Power take-off
RES	Residual gas fraction
RH	Relative humidity
SI	Spark ignition
USM	Universiti Sains Malaysia

a	Acoustic velocity
A	Area
A_r	Area ratio
ºC	Degree Celsius
ºCA	Degree crank angle
R	Gas constant
c	Gas particle velocity
m	mass
P	Pressure ratio (=p/p_o)
p	Pressure
γ	Specific heat ratio
T	Temperature
α	Wave propagation velocity

SIMULASI DAN UJIKAJI PENALAAN MASUKAN DAN EKZOS ENJIN AUTOMOTIF UNTUK PENAMBAHBAIKAN TORK PADA KELAJUAN RENDAH

ABSTRAK

Enjin kereta penumpang moden telah "dikecilkan saiz" untuk penjimatan bahan api, maka memerlukan putaran enjin yang tinggi untuk mendapatkan prestasi yang baik. Pengguna lebih gemar memperoleh tork pada putaran enjin rendah untuk pemanduan yang lebih baik. Enjin yang dikaji mempunyai 4 injap pada setiap silinder, 1.6 liter kapasiti, 2 profil sesondol masukan dan 2 ruang masukan yang berlainan panjang. Ia telah dimodel dan disahkan dengan prestasi enjin (kuasa, tork, dan lain-lain); dan tekanan dari kebuk pembakaran, ruang masukan dan ruang ekzos untuk menentukan tahap keyakinan ramalan model tersebut. Model ini kemudiannya dioptimumkan torknya pada putaran enjin rendah dengan memanipulasi konfigurasi dan panjang ruang ekzos; diameter dan panjang ruang masukan. Didapati bahawa sistem ekzos asal adalah terlalu pendek dan memberikan pengecasan ekzos yang tidak sekata di antara silinder. Keputusan simulasi menunjukkan bahawa peningkatan 2.7-5.6% dalam tork boleh direalisasikan dengan ruang ekzos yang panjang dan sistem ekzos yang mampu memberi pengecasan yang sekata di kalangan silinder. Peningkatan 2% tork boleh didapati dengan mengubah geometri ruang masukan kepada diameter yang lebih kecil. Enjin sasaran kemudiannya diubahsuai dengan ruang ekzos dan masukan. Keputusan menunjukkan peningkatan tork sebanyak 2.7-4.5% pada kelajuan enjin yang lebih rendah dengan penalaan ruang ekzos. Kesan penalaan ruang masukan tidak ketara tetapi ia menunjukkan arah kecenderungan yang serupa seperti yang ditunjukkan oleh simulasi..

SIMULATION AND EXPERIMENTAL STUDIES OF INTAKE AND EXHAUST TUNING FOR AUTOMOTIVE ENGINE LOW-END TORQUE ENHANCEMENT

ABSTRACT

Modern passenger car engines have been “down-sized” for improved fuel consumption, resulting in high speeds to obtain good performance. Consumers, however, are demanding improved low-end torque for improved drivability. The target engine; a 4 valve per cylinder, 1.6L engine with two intake cam profiles and 2 intake runner lengths, was modeled and correlated with measured engine performance characteristics (power, torque, etc.); and pressure traces from combustion chamber, intake and exhaust manifolds to establish the confidence level in the model's prediction. The model was then optimised for low-end torque by manipulating exhaust manifold configuration, exhaust runner length, intake diameter and intake runner length. It was found that the original exhaust system is too short and gives uneven exhaust cross-charging among the cylinders. Simulation result indicated that a 2.7-5.6% improvement in torque could be realised with an evenly cross-charged and longer exhaust runner. A 2% torque improvement was predicted by changing the intake manifold geometry to smaller diameter. The target engine was subsequently modified with new set of exhaust manifold and intake runner. Result showed a torque improvement of 2.7-4.5% at lower engine speed over the base design by exhaust tuning. Effect of intake tuning was not significant but it showed a similar trend as indicated by simulation.

CHAPTER 1 INTRODUCTION

1.1 Research Background

Internal combustion engine (ICE) technologies are likely to be the dominant power source for automobile for decades to come despite facing challenges from electric hybrids, electric powertrains, hydrogen fuel cell propulsion technology and etc. The higher cost and technological hurdles are the main reasons impeding the alternative systems to replace ICE for the time being (National Petroleum Council 2012). Among these, the hybrid system is the most likely to slowly replace ICE-only systems; and even then it still uses ICE technology.

During the time when fuel was cheap and car taxes were low, car manufacturers were not very concerned about engine efficiency, and as a result preferred bigger engines for more power. The development cost of bigger engines was less compared to doing research and development to improve the performance of smaller and more efficient engines (Baker 2002). However, due to fluctuations in fuel prices and higher taxes imposed on vehicle, many people opt to buy smaller and more efficient vehicles to reduce the transportation costs.

In Malaysia, present (year 2014) selling price of RON95 petrol cost RM2.10 compared to RM 1.20 of RON97 petrol in year 2000. The Malaysian government also imposes higher tax rate on bigger vehicles to compensate for the impact of such vehicles on the environment. According to Table 1.1, annual road tax rates for vehicles with engine capacity higher than 1600cc are about double the road taxes of vehicles with engine capacity less than 1600cc. Excise duty for imported motor cars above 2500cc are also higher i.e. 105% compared to 75% for vehicle less than 1800cc (Malaysia Automotive Association n.d.).

Table 1.1: Road tax rate of individually owned motocar in Peninsular Malaysia

Engine capacity (cc)	Road tax rate
< 1,000	RM20
1001 – 1200	RM55
1201 – 1400	RM70
1401 – 1600	RM90
1601 – 1800	RM200.40 to RM280
1801 – 2000	RM280.50 to RM380
2001 – 2500	RM381 to RM880
2501 – 3000	RM882.50 to RM2130
3001 – 5000	RM2134.50 to RM11130

Source: Jabatan Pengangkutan Jalan Malaysia 2009

Another challenge faced by vehicle manufacturers is the emission standard where the new vehicle models must not exceed the limit of the amount of pollutants that can be released into the environment. Engine downsizing is recognised to be one of the most effective ways to reduce CO_2 emission and to meet the regulations (Pallotti et al. 2003) (Lecointe & Monnier 2003).

Engine downsizing is the reduction of engine capacity by using smaller displacement engine. Smaller engine will have lower fuel consumption hence reduced CO_2 emission. Other than that, smaller engine will have lower pumping loss and friction loss which contribute to better engine efficiency (Pagot et al. 2006). However, output power of downsized engine needs to be remained for the satisfaction of consumer; hence air boosting technique such as supercharging or turbocharging is the solution to gain back the power. Engine downsizing can reduce emissions by 10% when compared to the base engine (Arif Basheer 2010).

Consumer requirements of low vehicle operating cost along with the need to comply with legal regulations will likely result in an increase in the sales of small, efficient vehicles. Figure 1.1 shows that more than 60% of cars in Europe in year 2009 were less than 1600cc and Frost & Sullivan predicted that the figure will go up to 80% by the year 2016.

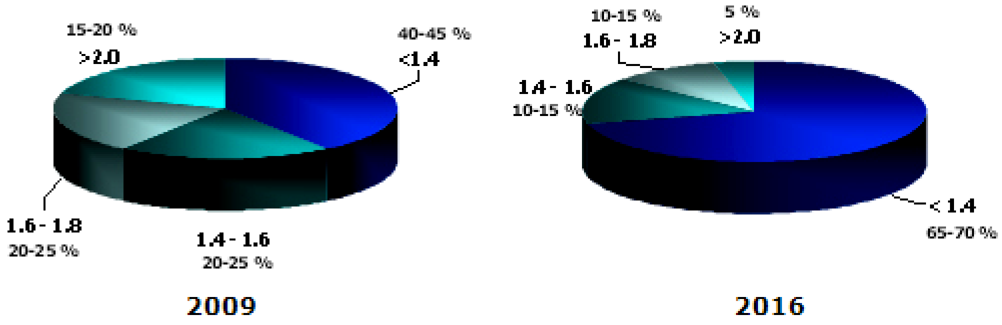

Figure 1.1: Share of gasoline engines' displacement ranges in liters (Arif Basheer 2010).

1.2 Low-End Torque

However, small engines require high speeds to obtain good performance. Most of them produce peak power at engine speeds above 6000rpm and peak torque at engine speeds above 4000rpm as shown in 0. Consumers are demanding better low-end torque as automotive SI engines run under low load and low speed under most of the driving conditions (França 2009). Consumers also request for improved drivability i.e. smoothness of power delivery during cruising and mild acceleration that fall into lower engine speed range. Based on the specifications of the target engine in this research (i.e. Campro CPS engine in Proton Exora), calculations based on the gear ratio show that the engine rotates at ≈2500-3250rpm when cruising at highway speeds as in Table 1.2.

Table 1.2: Proton Exora engine speed at corresponding vehicle speed

Vehicle speed	A/T engine speed	M/T engine speed
90km/h	2478rpm	2669rpm
110km/h	3029rpm	3263rpm

The most efficient operating point for SI engines is at lower engine speed as shown in brake specific fuel consumption (BSFC) contour in Figure 1.2. The performance map shows that 2000-3000rpm part load is the most efficient operating point of a 4 cylinders SI engine. This is due to the lower piston speed which results in lower engine friction compared to high speed operation (Heywood 1988). Other than the major friction contribution by piston assembly, frictions from crankshaft, valve train and other accessories also decrease at lower engine speeds as shown in friction breakdown curves in Figure 1.3

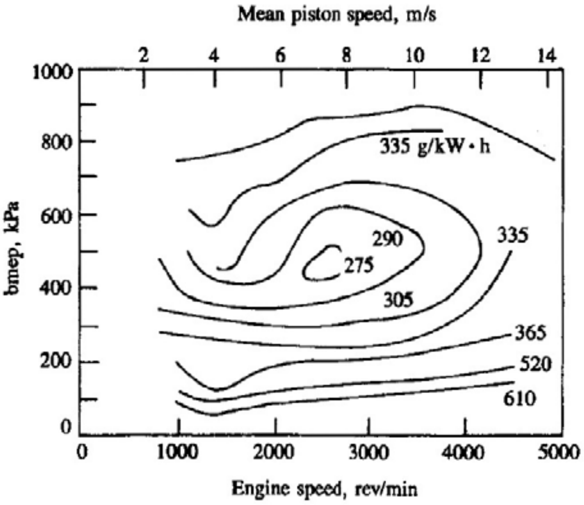

Figure 1.2: Performance map for 2 liter 4 cylinders SI engine (Heywood 1988).

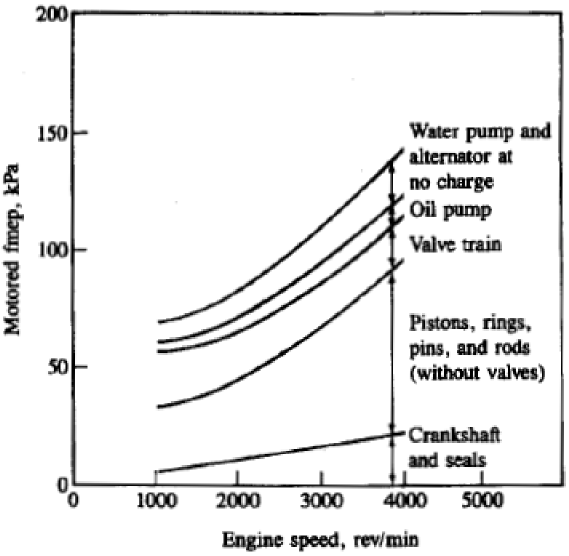

Figure 1.3: Motored FMEP vs. engine speed of a 4 cylinders SI engine (Heywood 1988).

Automotive engines with good low-end torque will have the advantage of:

i. better drivability, i.e. smooth power delivery at cruising and acceleration
ii. better torque at most common operating point
iii. operating at better efficient point hence lower fuel consumption

1.3 Problem Statement

Due to the increasing operating cost of personal transportation especially on bigger capacity vehicle, consumers tend to buy smaller capacity passenger cars. Car manufacturers tend to produce smaller vehicle for legal compliance. These have lead to the trend of owning small and efficient vehicles. Engine downsizing, i.e. smaller displacement engine along with turbocharger is the best solution.

However, turbocharging has the drawback on low-end torque and turbo lag (Pagot et al. 2006) (Pallotti et al. 2003). Small engines also have their peak performance at high speeds while the consumers are demanding greater low-end torque for fuel economy and better drivability.

Low-end torque of the naturally aspirated small automotive engine will be focused in the research. It can serve the need of market and can be a good base engine for turbocharging that encounters turbo lag and less effective at low-end.

1.4 Objectives

The objectives of this research are as follow:

i. To develop a validated engine model and perform parametric study to improve the low-end performance of a 4-stroke 4 cylinders spark ignition engine.
ii. To modify the test engine for low-end torque enhancement and test the performance on a dynamometer.

1.5 Scope of Research

The scope of this research is as follows:

i. Setting up a workable test cell with proper instrumentation systems such as dynamometer controller, data acquisition system, pressure sensor and etc.
ii. Engine performance tests in order to have baseline data for analysis and to be used as input to the engine model.
iii. Develop an engine model by using Ricardo WAVE 1-D engine and gas dynamics simulation software; and validate the model with experimental data.

iv. Using the engine model to analyse the low-end performance of the original engine and perform parametric study to improve the low-end torque of the engine.

v. Modify the engine according to result of parametric study and test the final performance of modified engine on dynamometer.

CHAPTER 2 LITERATURE REVIEW

2.1 Overview

This Chapter starts with few methods that could improve low end performance of a SI automotive engine. Then manifold tuning is discussed in detail which includes the background of manifold tuning, pressure wave's nature and its gas dynamic effect, followed by the principle of intake and exhaust tuning on four-stroke engine.

2.2 Solutions for Low-End Torque

There are several ways to improve low-end performance of an automotive engine such as forced induction, valve timing and profile adjustment and manifold tuning.

2.2.1 Forced Induction

Supercharging and turbocharging are power boosting techniques which supply compressed higher density air to the engine. The maximum power of an engine is limited by the amount of fuel which can be efficiently burnt in the engine. The amount of fuel is limited by the amount of air being inducted to the engine based on the engine management system's air fuel ratio setting. By pressurising the inlet air, the mass flow rate of air increases and the corresponding fuel flow also increases. This leads to the increment of power output of the engine (Stone 1999). Eqn. (2.1) shows how the power, P of a 4-stroke engine is affected by inlet air density, $\rho_{a,i}$ (Heywood 1988):

$$P=\frac{\eta_f \eta_v N V_d Q_{HV} \rho_{a,i}(F/A)}{2} \tag{2.1}$$

Where:

η_f is fuel conversion efficiency

η_v is volumetric efficiency

V_d is displacement volume

N is crankshaft rotational speed

Q_{HV} is heating value of fuel

F/A is fuel air ratio

In a supercharger, part of the engine output power is used to turn the compressor hence there will be fuel consumption penalty in the system. In a turbocharger, energy from exhaust stream is used to turn the turbine which is connected to a compressor through a common shaft to provide the compressed air. Therefore turbocharging is more efficient because it uses the energy available in exhaust waste heat to run the turbine-compressor. However, transient response or turbo lag is one of the challenges in turbocharging as time is needed for the exhaust gas to accelerate the turbine to generate increased boost (Gurney 2001) (Hamilton et al. 2009). A variable geometry turbocharger is a good solution for better low-speed torque and to reduce the turbo lag effect but there will be a challenge to introduce this in a low cost gasoline engine (Frost & Sullivan 2012).

These power boosting techniques are more challenging in spark ignition (SI) engines compared to compression ignition (CI) engines due to the wider air flow range (due to wider speed range and throttling) and require more careful control to prevent knock occurring (Stone 1999). Knock tendency is higher when high end-gas pressure and temperature exist in the combustion process. Tubocharging or supercharging a SI engine will increase the inlet air pressure and temperature which in turn gives higher end-gas pressure and temperature. Often, operating parameters of a turbocharged SI engine are adjusted to reduce the knock impact. Lower compression ratio, richer air fuel ratio and retarded spark timing are common approaches to deal with knock problem but all these approaches will have a negative impact on fuel efficiency and prevents the full potential of boosting being realised in SI engines. Their usage is more common in diesel engines because they do not have knock issues (Heywood 1988).

2.2.2 Valve Timing and Lift Profile

Valves and ports are the flow restrictions in intake and exhaust systems of a 4-stroke engine. Therefore valve timing and lift profile play an important role in engine performance by regulating the air flow into and out from the cylinder in order to have better gas exchange process and maximise volumetric efficiency. However, it can only optimise the performance at particular engine speed and will compromise power over the rest of the speed range. Hence considerable effort has been devoted to develop variable valve timing (VVT) mechanisms to minimise the valve timing compromises (Stone 1999).

VVT mechanisms alter the valve events so that the engine can be tuned for different engine speed range. Common VVT mechanisms include valve event phasing (opening and closing events are moved equally) and switching between 2 different cam profiles. Perodua Viva and Myvi DVVT systems feature the valve event phasing mechanisms on intake valves while Proton Campro CPS engine features switching mechanism between 2 different cam profiles on intake camshaft. The best VVT system would be the "camless engine" which uses electromagnetic, hydraulic, or pneumatic actuators to open the valves; hence any profile could be obtained at any speed range. However the camless system has its challenges such as accuracy at high speed, weight and packaging issues, high cost, and unsafe operation in case of electrical problems.

The targeted engine in this research, Campro CPS engine features cam profile switching mechanism where low lift cam will switch to high lift cam at high engine speed (section 3.2). This allows us to modify the low lift cam profile to further improve low end torque. However, altering the cam profile was not considered in this research due to the high cost and availability of the service locally.

2.2.3 Manifold Tuning

Engine performance can also be enhanced by gas dynamic effects in the manifolds, i.e. pressure wave charging method via pulse originating from valves opening and closing movements. When the valves open, a pressure wave (either compression or expansion) is generated and moves in the intake or exhaust manifold until it meets the other end or meets a junction; and is then reflected back. If the manifold length is tuned correctly, a reflected compression wave will arrive at the intake valves shortly before intake valves close (IVC), increasing the amount of air being inducted into cylinder. Correspondingly, an expansion wave arriving at exhaust valves during valve overlap period will create a positive scavenging gradient relative to intake manifold and aid in the expulsion of residual gas (Hiereth & Prenninger 2007). The length of the manifold will determine the engine speed which obtains the maximum benefits from the pulsating flow.

Campro CPS engine features VIM (variable length intake manifold) that takes advantage of the different reflection lengths to improve engine performance at different speed ranges. This allows us to improve low end performance by tuning the geometry of intake system of lower engine speed range.

2.3 Manifold Tuning Background

As the pressure wave action is defined by the periodic nature of intake and exhaust processes, the gas exchange process is extremely dependent on engine speed. Therefore it is possible to tune the engine manifold to have specific power characteristic as a function of speed. An example of manifold tuning is that a given 2.0 liter natural aspirated engine might be used in a normal passenger car, a sports car, a multipurpose vehicle (MPV), and in a 4 wheel drive (4WD) vehicle each with a separate tuning. While new engines might not be designed very often, manifold redesign becomes important to cater for these different requirements from the only engine (Winterbone & Pearson 2001).

It has been long known that the manifold design has large effect on engine performance. However, induction tuning of a SI engine was severely constrained until the introduction of multipoint fuel injection system. Carburetted or single-point fuel injection system delivers fuel to the upstream of manifold; has high tendency to form fuel films along the manifold wall (Winterbone & Pearson 2001). Due to the geometric variation of each runner, air fuel ratio in each cylinder will vary. Multipoint fuel injection or port fuel injection system injects fuel to the intake port of each cylinder to precisely control the mixture strength delivered to the cylinders. With this technology, fuel no longer is transported from throttle body through the entire manifold. Manifold design can be optimised for air flow alone to create ramming or tuning effect without having the fuel flow constraint (Heywood 1988).

Manifold tuning for low end torque can have the advantage of having longer gear ratio in the transmission so that the engine operates at lower speed while maintaining the same vehicle speed. With this, engine friction and pumping losses are lower and thus the engine operates with better fuel efficiency.

2.4 Pressure Wave

Pressure waves are of either compression waves or expansion waves. Some of the literatures describe compression waves as compression pulses, exhaust pulses or ramming waves. Expansion waves are often called as rarefaction waves, suction pulses, sub-atmospheric pulses or intake pulses (Blair 1999).

Pressure wave's motion will be discussed in this section; followed by the reflection of pressure waves at junctions. The purpose of this is to give an overview of the nature of pressure wave's in engine manifold.

2.4.1 Pressure Wave's Motion in Pipe

Figure 2.1(a) shows compression pressure wave that travels toward the right having pressure of p_e which has magnitude higher than atmospheric pressure p_o. The compression wave propagates at the velocity of α_e while the gas particles move in the same direction at velocity of c_e. This situation is similar to the exhaust blowdown process at the moment when exhaust valves open. Exhaust blowdown creates a compression wave towards exhaust runner while the exhaust gas flows in the same direction.

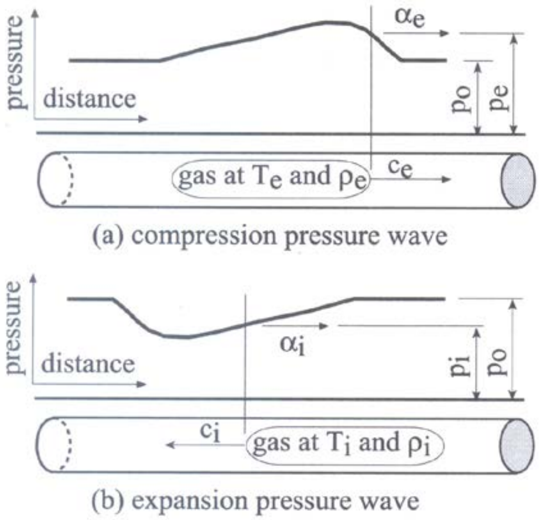
pressure
distance
αe
po
pe
gas at Te and ρe
ce
(a) compression pressure wave
pressure
distance
αi
pi
po
ci
gas at Ti and ρi
(b) expansion pressure wave

Figure 2.1: Pressure waves propagation in pipe (Blair 1999).

Expansion pressure wave in Figure 2.1(b) at pressure p_i (lower magnitude than p_o) propagates at velocity α_i towards the right. The gas particles move at gas particle velocity of c_i but in opposite direction of the wave propagation. This situation is similar to intake process when the intake valves open, piston downward motion create a suction wave to the intake runner then the plenum while the fresh air flows into the cylinder direction.

2.4.2 Wave Propagation Velocity and Gas Particle Velocity

Absolute propagation velocity, α of any point on a wave is the sum of local acoustic velocity, a and the local gas particle velocity, c:

$$\alpha=a+c \tag{2.2}$$

Assuming the process is isentropic,

$$\frac{T}{T_o}=\left(\frac{p}{p_o}\right)^{\frac{\gamma-1}{\gamma}}=(P)^{\frac{\gamma-1}{\gamma}} \tag{2.3}$$

P is pressure ratio, i.e. p/p_o. Then,

$$\frac{a}{a_o}=\frac{\sqrt{\gamma RT}}{\sqrt{\gamma RT_o}}=\sqrt{\frac{T}{T_o}}=P^{\frac{\gamma-1}{2\gamma}} \qquad (2.4)$$

Earnshaw (1860) and Bannister (1958) (cited in Blair 1999) showed the gas particle velocity, c as:

$$c=\frac{2a_o}{\gamma-1}\left(P^{\frac{\gamma-1}{2\gamma}}-1\right) \qquad (2.5)$$

By substituting eqn. (2.4) and eqn. (2.5) into eqn. (2.2),

$$\alpha=a+c=a_oP^{\frac{\gamma-1}{2\gamma}}+\frac{2a_o}{\gamma-1}\left(P^{\frac{\gamma-1}{2\gamma}}-1\right)=a_o\left[P^{\frac{\gamma-1}{2\gamma}}\left(\frac{\gamma+1}{\gamma-1}\right)-\frac{2}{\gamma-1}\right] \qquad (2.6)$$

Reference acoustic velocity, a_o is defined as:

$$a_o=\sqrt{\gamma RT_o} \qquad (2.7)$$

Let say the pressure wave travels in undisturbed air of standard atmospheric condition, i.e. 101.325kPa and 293K; the reference acoustic velocity, a_o is:

$$a_o=\sqrt{\gamma RT_o}=\sqrt{1.4\times287\times293}=343.1\text{m/s} \qquad (2.8)$$

i. **Compression Wave**

For a compression wave of pressure ratio, P of 1.2 that travels in undisturbed air, the gas particle velocity, c and wave propagation velocity, α are as below:

$$c=\frac{2a_o}{\gamma-1}\left(P^{\frac{\gamma-1}{2\gamma}}-1\right)=\frac{2\times343.1}{1.4-1}\left(1.2^{\frac{1.4-1}{2\times1.4}}-1\right)=45.3\text{m/s} \qquad (2.9)$$

$$\alpha=a_o\left[P^{\frac{\gamma-1}{2\gamma}}\left(\frac{\gamma+1}{\gamma-1}\right)-\frac{2}{\gamma-1}\right]=343.1\left[1.2^{\frac{1.4-1}{2\times1.4}}\left(\frac{1.4+1}{1.4-1}\right)-\frac{2}{1.4-1}\right]=397.4\text{m/s} \qquad (2.10)$$

The compression wave at velocity 397.4m/s is moving faster than reference acoustic velocity, a_o while the air particle is moving at slower speed of 45.3m/s in the same direction.

ii. Expansion Wave

For an expansion wave of pressure ratio, P of 0.8 that travels in undisturbed air, the gas particle velocity, c and wave propagation velocity, α are as follows:

$$c=\frac{2a_o}{\gamma-1}\left(P^{\frac{\gamma-1}{2\gamma}}-1\right)=\frac{2\times343.1}{1.4-1}\left(0.8^{\frac{1.4-1}{2\times1.4}}-1\right)=-53.8\text{m/s} \tag{2.11}$$

$$\alpha=a_o\left[P^{\frac{\gamma-1}{2\gamma}}\left(\frac{\gamma+1}{\gamma-1}\right)-\frac{2}{\gamma-1}\right]=343.1\left[0.8^{\frac{1.4-1}{2\times1.4}}\left(\frac{1.4+1}{1.4-1}\right)-\frac{2}{1.4-1}\right]=278.5\text{m/s} \tag{2.12}$$

The expansion wave at velocity 278.5m/s is moving slower than reference acoustic velocity, a_o while the air particle is moving at slower speed of 53.8m/s at the opposite direction (- sign).

2.5 Pressure Wave Reflection

Pressure waves reflect at boundaries of the inlet or exhaust duct such as open or closed end of a pipe, a sudden or gradual change in flow area and pipe branches. Any of these reflections would initiate a superposition process as the reflected waves move oppositely to the incident pressure waves. A simple example of pressure wave reflection is echo caused by sound reflection on a closed end surface.

This section will focus on the various reflection phenomena that might occur in an engine manifold due to changes in duct geometry. The purpose is to illustrate the wave reflection mechanism in internal combustion engines for better understanding. The discussions are far from complete description of the processes and are based on simple equations with some assumption which might give inaccurate mass flow rate at certain cases but it serve as good overview of how the pressure waves reflect or change its form when encounter junctions.

2.5.1 Pressure Wave Reflection at the Open End of a Pipe

The main feature of a simple open end boundary is that the pressure at pipe exit is equal to the atmospheric pressure, i.e. reference pressure, p_o. A pressure wave reflected at an open end is reversed thus an incident compression wave is reflected as an expansion wave at the open end of pipe, and vice versa (Winterbone & Nichols 1985). The isometric distance-time pressure diagram in Figure 2.2 shows the reflection of an incident compression wave at the open pipe end results in a reflected expansion wave.

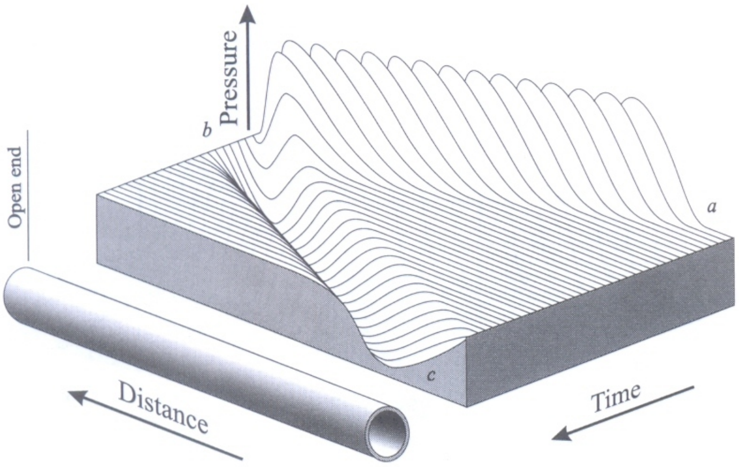

Figure 2.2: Pressure wave reflection at open end (Winterbone & Nichols 1985).

2.5.2 Pressure Wave Reflection at the Closed End of a Pipe

There is no flow transmitted at the closed end boundary, hence the velocity at the closed end is zero. The reflected wave at closed end boundary is the same and equal magnitude as incident wave. This is because there is no flow at the closed end and the incident wave must be sent back. This is shown in Figure 2.3. The reflection of wave at b results in an increment of pressure, which is caused by the momentum reversal of the wave (Winterbone & Nichols 1985).

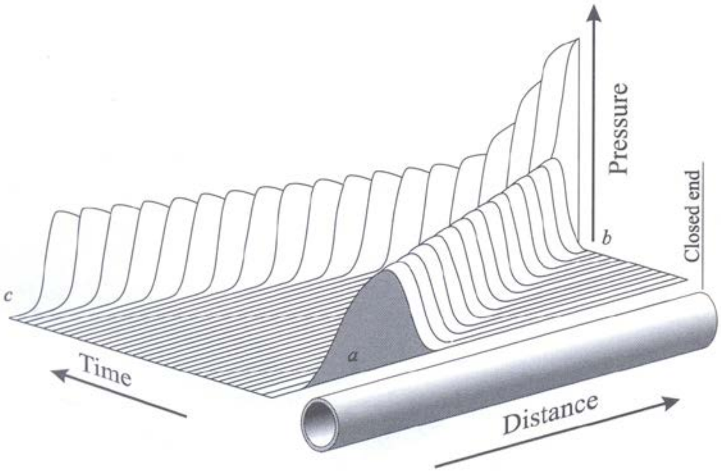

Figure 2.3: Pressure wave reflection at closed end (Winterbone & Nichols 1985).

2.5.3 Pressure Wave Reflection at Sudden Area Change

From gas dynamic standpoint, a sudden change in pipe area may be considered as a 1-dimensional problem. For a pressure wave that propagates through an area change within a duct, change in amplitude of the transmitted pulse and a reflection of wave occur.

Figure 2.4 shows the sudden area change schematic diagram. Subscript "1" and "2" represent the upstream and downstream of area change; "i" is the incident pulse where "r" is the reflected pulse; and "s" is the superposition condition.

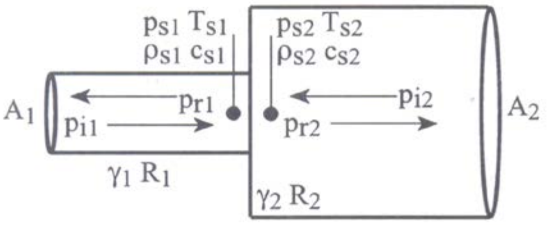

(a) sudden expansion in area in a pipe where $c_S > 0$

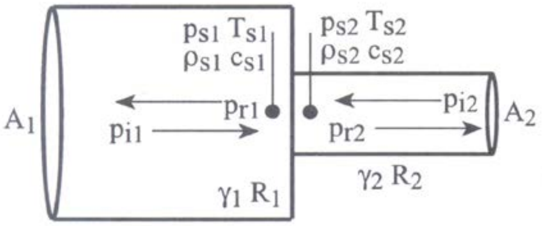

(b) sudden contraction in area in a pipe where $c_S > 0$

Figure 2.4: Sudden expansion and sudden contraction in pipe flow (Blair 1999).

Benson suggested a simple theoretical solution for such junctions. He assumed that the process is isentropic and the superposition pressure, p_s at the junction is the same in both pipes i.e. $p_{s1}=p_{s2}$ (Benson 1982). Such assumption may have its limitation but Blair claimed that it is effective if the area ratio, A_r is in the range of $1/6 < A_r < 6$. Based on Benson's simple "constant pressure" assumption, the reflected wave's pressure ratio, P_r are:

$$P_{r1}=\left(\frac{(1-A_r)P_{i1}^{\frac{\gamma-1}{2\gamma}}+2A_rP_{i2}^{\frac{\gamma-1}{2\gamma}}}{1+A_r}\right)^{\frac{2\gamma}{\gamma-1}} \tag{2.13}$$

$$P_{r2}=\left(\frac{2P_{i1}^{\frac{\gamma-1}{2\gamma}}-(1-A_r)P_{i2}^{\frac{\gamma-1}{2\gamma}}}{1+A_r}\right)^{\frac{2\gamma}{\gamma-1}} \tag{2.14}$$

Lets consider examples of sudden enlargement of $A_r = 2$ and sudden contraction of $A_r = 1/2$; incident wave at upstream is either compression wave of pressure ratio, $P_i = 1.2$ or expansion wave of $P_i = 0.8$. The downstream incident wave is still air, hence $P_{i2} = 1$. The gas involved is air and the specific heat ratio, $\gamma = 1.4$.

i. Compression Wave at Sudden Enlargement

For a compression wave of pressure ratio 1.2 that propagate through a sudden enlargement of double the flow area, $A_r = 2$; the transmitted wave into downstream pipe 2 is in compression with reduced pressure ratio of $P_{r2} = 1.13$. The reflected wave towards the upstream pipe 1 is an expansion wave at $P_{r1} = 0.94$.

ii. Expansion Wave at Sudden Enlargement

For an expansion wave of pressure ratio 0.8 that propagate through a sudden enlargement of double the flow area, $A_r = 2$; the transmitted wave into downstream pipe 2 is in expansion with diminish pressure ratio of $P_{r2} = 0.862$. The reflected wave towards the upstream pipe 1 is a compression wave at $P_{r1} = 1.076$.

iii. Compression Wave at Sudden Contraction

For a compression wave of pressure ratio 1.2 that propagate through a sudden contraction of half the flow area, $A_r = 1/2$; the transmitted wave into downstream pipe 2 is in compression with increased pressure ratio of $P_{r2} = 1.274$. The reflected wave towards the upstream pipe 1 is also compression wave at $P_{r1} = 1.063$.

iv. Expansion Wave at Sudden Contraction

For an expansion wave of pressure ratio 0.8 that propagate through a sudden contraction of half the flow area, $A_r = 1/2$; the transmitted wave into downstream pipe 2 is in stronger rarefaction wave with pressure ratio of $P_{r2} = 0.741$. The reflected wave towards the upstream pipe 1 is also a rarefaction wave but weaker magnitude, i.e. at $P_{r1} = 0.929$.

Benson theory is clearly too simple to be accurate in all circumstances but it is a very good guide to determine the magnitude of transmitted and reflected wave. A more theoretical approach that does not assume constant pressure at discontinuity of sudden area change and considers the flow at sudden expansion as non isentropic process as the expanding flow will leave turbulent vortices and give rise to particle flow separation. This approach is highly iterative and requires a computer to solve the equations. Blair has done a comparison between the constant pressure theory and the more complex theory. The results showed that the error between the air mass flow rate between these two theories is less than 10%, i.e. 0.3% error for sudden expansion and 9.1% for sudden contraction case (Blair 1999).

2.5.4 Pressure Wave Reflection at Branches of Pipe

There are two approaches for multi-pipe junctions, i.e. constant pressure and the pressure loss approaches. Constant pressure assumption is acceptable for diesel engine simulations because of the lower flow velocity in diesel engine. For gasoline engines, gas flow velocity is higher and the pressure loss at the junction become significant as this is going to affect the engine volumetric efficiency (Winterbone & Pearson 2000).

Similar with sudden area change, Benson suggested that the superposition pressure at all pipe ends of the branch is uniform, i.e. $P_{s1} = P_{s2} = ... = P_{sn}$. The process is assumed to be isentropic (Benson 1982). A sketch of 3-way branch is shown in Figure 2.5. Any inward propagation of pressure wave towards the branch is regarded as "positive" and vice versa.

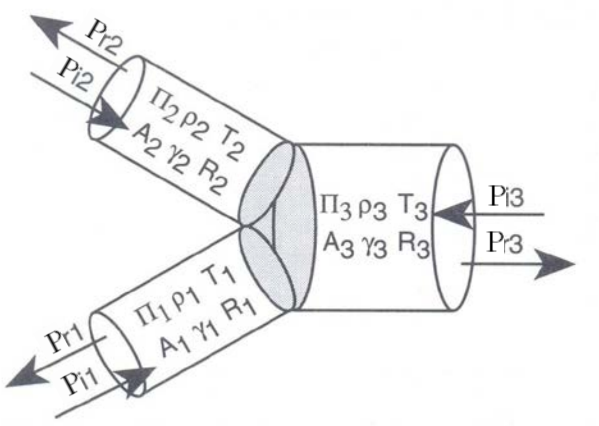

Figure 2.5: Pressure wave propagation at 3-way branch (Blair 1999).

Based on the assumption above, reflected wave's pressure, P_r are as below:

$$P_{r1}=\left(\frac{2A_2P_{i2}^{\frac{\gamma-1}{2\gamma}}+2A_3P_{i3}^{\frac{\gamma-1}{2\gamma}}+P_{i1}^{\frac{\gamma-1}{2\gamma}}(A_1-A_2-A_3)}{A_t}\right)^{\frac{2\gamma}{\gamma-1}} \tag{2.15}$$

$$P_{r2}=\left(\frac{2A_1P_{i1}^{\frac{\gamma-1}{2\gamma}}+2A_3P_{i3}^{\frac{\gamma-1}{2\gamma}}+P_{i2}^{\frac{\gamma-1}{2\gamma}}(A_2-A_3-A_1)}{A_t}\right)^{\frac{2\gamma}{\gamma-1}} \tag{2.16}$$

$$P_{r3}=\left(\frac{2A_1P_{i1}^{\frac{\gamma-1}{2\gamma}}+2A_2P_{i2}^{\frac{\gamma-1}{2\gamma}}+P_{i3}^{\frac{\gamma-1}{2\gamma}}(A_3-A_2-A_1)}{A_t}\right)^{\frac{2\gamma}{\gamma-1}} \tag{2.17}$$

Where:

A_t is total area, i.e. $A_1 + A_2 + A_3$

Let's look at some simple examples of 3-way branch to understand how the pressure wave propagation at multi-pipe junction. For simplicity, all of the pipes are of equal area and the gases involved are air only.

i. Compression Wave Arriving at one of the Pipes

An incident compression wave of pressure ratio, P_{i1} = 1.2 originated from pipe 1 and the condition of the other 2 pipes undisturbed, i.e. P_{i2} = P_{i3} = 1. The outcome is similar to sudden expansion. Compression wave are transmitted to pipe 2 and 3 at pressure ratio, P_{r2} = P_{r3} = 1.13. Expansion wave of P_{r1} = 0.94 is reflected back into pipe 1.

ii. Compression Waves Arriving at Two of the Pipes

Incident compression waves of pressure ratio, P_{i1} = P_{i2} = 1.2 from pipe 1 and pipe 2 move toward the 3-way branch. The condition of the pipe 3 is undisturbed, i.e. P_{i3} = 1. The outcome is similar to sudden contraction. Compression wave is transmitted to pipe 3 at increased pressure ratio of P_{r3} = 1.274. Reflected waves back into pipe 1 and 2 are also compression waves but at weaker pressure ratio, P_{r1} = P_{r2} = 1.0632.

Constant pressure assumption does not account the angles between the pipes at the branch. Whenever there is a change in flow direction when moving through the branch, there must be some pressure loss with entropy gains (Fleck et al. 1998). Again, the complete solution that considers the pressure loss and entropy gain is highly iterative and requires the computer to solve the equation. According to Blair's (1999) comparison of these 2 approaches, the amplitudes of the reflected pressure waves are quite similar but more serious errors occur in the mass flow rate calculation.

2.6 Intake Tuning

During the intake stroke, piston descends and creates a low pressure region in the cylinder. This generates an expansion wave that propagates to the intake pipe. When the expansion wave reaches the plenum; a bigger volume junction, it reflects back to the inlet valves as compression wave as if pressure reflection at the sudden expansion junction. If the arriving of a compression wave at intake valves is at the short period before intake valve closing, IVC, the intake mass flow rate into the engine can be boosted. Intake pressure before IVC is the dominant effect in intake tuning (Sammut & Alkidas 2007).

Ohata and Ishida showed that the volumetric efficiency of an engine is highly influenced by the pressure at the inlet valve before the IVC (Ohata & Ishida 1982). The volumetric efficiency, η_v is approximated by:

$$\eta_v=\eta_{vo}+Cp_m \tag{2.18}$$

Where:

η_{vo}	the volumetric efficiency if pressure at the inlet valve is atmospheric
C	ramming coefficient
p_m	mean pressure in the significant period, i.e. 50 degrees before IVC

Therefore, the objective of intake tuning is to provide high pressure at IVC to improve the volumetric efficiency.

Vitek and Polasek (2002) claimed that it was confirmed that by computation as well as by measurement that it is better to have pressure peak at the end of the intake stroke. A computational result of optimal intake length (that give best output power) at each engine speed is shown in Figure 2.6. All the curves show peak pressure before IVC. Some of the pressure curves were noticed to have pressure back flow but yet still give the best output power. This shows that pressure peak before IVC is more significant than peak pressure at IVO.